ACS OMEGA

http://pubs.acs.org/journal/acsodf

Article

Antibacterial Activity Studies of 3D-Printing Polyetheretherketone Substrates with Surface Growth of 2D TiO_2/ZnO Rodlike Arrays

Ngi-Chiong Lau, Yin-Cheng Lai, Dave W. Chen,* and Kong-Wei Cheng*

Cite This: *ACS Omega* 2022, 7, 9559−9572

Read Online

ACCESS | Metrics & More | Article Recommendations | Supporting Information

ABSTRACT: Heterogeneous metal implants have been applied in clinical treatments of skeletal wounds, but their low antibacterial properties and the possibility of a release of metal ions may have harmful influences on the human body. Therefore, a polymer implant with low cost, high safety, an elastic modulus similar to that of human bone, and a good antibacterial property must be produced for orthopedic treatments. In this study, the surface of a 3D-printed polyetheretherketone (PEEK) disk was grown with ZnO/TiO_2 rodlike arrays using a chemical bath deposition. X-ray diffraction patterns and transmission electron microscopy images showed that TiO_2/ZnO rodlike arrays were deposited onto the PEEK substrate. With the direct absorption of antibiotic agents onto the surface of TiO_2/ZnO/PEEK samples, their antibacterial performances greater than the values of minimum inhibitory concentration required to inhibit the growth of 90% of *Escherichia coli* (*E. coli*) and *Staphylococcus aureus* (*S. aureus*) remained for around 10 days. The concentration of Zn^{2+} ions in a buffer solution is reduced with the coating of a TiO_2 layer on a ZnO rodlike array. The sample with absorption from a mixture containing ampicillin and vancomycin salts with a weight ratio of 1:1 had the best inhibitory effect on the growth of *E. coli* and *S. aureus*.

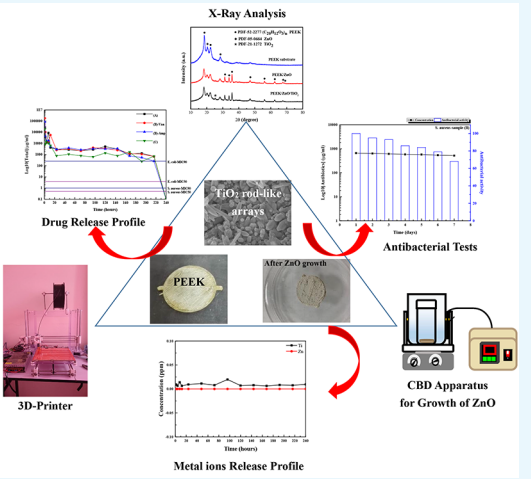

1. INTRODUCTION

With the fast increase in industrialization and population around the world, a decrease in manufacturing time for mechanical processes is necessary. Recently, a new technology called 3D-printing has been developed and applied in the industrial field due to it having low cost, simple procedures, and short manufacturing time compared with traditional mechanical processes. For Wohlers Report published by Campbell et al. (2018),[1] industrial applications using 3D-printing technology will increase to around 22 billion US dollars in 2022. Major applications using 3D-printing technology include discrete manufacturing and medical, food, aerospace, and biological technologies.[2] For applications in fields related to medicine and biology, 3D-printing techniques have been employed because of the difficult production of complex structures for bone supports.[3] Various types of 3D-printing technologies such as stereolithography appearance (SLA), fused deposition modeling (FDM), and selective laser sintering (SLS) have been reported in the literature.[2,4−6] Traditional metal-based materials such as Ti-based metal junctions or supports are often applied in the clinical treatments of complex skeletal wounds. However, major issues for the treatments of these skeletal wounds using Ti-based supports are metal ions released from metal implants caused by corrosion in the human body and the mismatched elastic moduli between human bone (7−30 GPa) and the metal implant (∼110 GPa for the Ti-based metal support).[2,7,8] Another candidate material applied in clinical surgeries involving complex skeletal wounds is semicrystalline polymer such as polyetheretherketone (PEEK).[2,7,8] PEEK has been applied in bone or tissue engineering due to its good elastic modulus (3−4 GPa), which is close to that of human bone (7−30 GPa).[2,7−9] Compared with traditional metal-based implants, an implant made with PEEK has several advantages such as an elastic modulus similar to that of human bone, low stress shield, and good thermal and chemical properties. Its elastic modulus that is similar to human bone and its low stress shield result in an enhancement in the lifespan of implants and a mechanical compatibility better than that of Ti-based metal supports. Its good thermal and chemical properties are also suitable for applications in the orthopedic treatments.[10−13] Although 3D-printing technology has been applied in orthopedic treatments such as total knee replacement or total hip replacement surgeries, implant-associated infection

Received: December 7, 2021
Accepted: February 24, 2022
Published: March 7, 2022

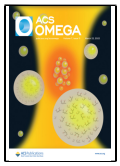

https://doi.org/10.1021/acsomega.1c06931
ACS Omega 2022, 7, 9559−9572

(IAI) is still a major problem in clinical surgeries involving these complex skeletal wounds. The ratios of IAIs for fracture-fixation, total hip replacement, and total knee replacement surgeries are 5%, 1%, and 2%, respectively.[14] These IAI ratios will increase exponentially for immunocompromised patients, and therefore, it is necessary to perform revision surgeries. However, the infection ratios for these revision surgeries can increase to values in the range 5−40%.[15] IAIs are difficult to treat and lead to extensive morbidity and even mortality. Moreover, orthopedic treatments of these complex skeletal wounds with implants always result in periprosthetic joint infection (PJI),[16] which is caused by *Staphylococcus aureus* or Gram-negative bacteria.[17] A general surgery for PJI involves the local delivery of a high concentration of antibiotic agent. The delivery of a high concentration of antibiotic agent into the desired region in the human body may lead to drug waste and generate cytotoxicity in cells in the human body.[18] Therefore, maintaining a heterogeneous implant with long and good antibacterial activity is an important issue for the care of patients after surgical operations. The development and improvement of these implants with long and good antibacterial properties have thus become a new research direction for orthopedic treatments. Hassan et al. (2013)[19] discussed various techniques for the modification or improvement of these implants with suitable antibacterial properties. Current research topics for the modification of these implants with suitable antibacterial properties include the coating of a thin film containing silver ions at the sample surface, surface polymerization of the antimicrobial material, and the production of some suitable functional groups at the implant surface using plasma or polymerization treatments. However, coating with a thin film containing transitional heavy metal ions onto the implant surface may also cause some unknown problems in clinical treatments. Another possible technique is the coating of a thin film containing a mixture with biodegradable polymer and antibiotic agents onto the surface of these heterogeneous implants to reduce the possibility of infection. A thin film with biodegradable polymer and antibiotic agents coated onto the surface of an implant can maintain a stable and local antibiotic agent transportation pathway to reduce the possibility of infection of the skeletal wounds. A polymer such as poly-lactic-*co*-glycolic acid (PLGA) mixed with an appropriate concentration of an antibiotic agent, which can be released at a maintained, stable release rate, is thus employed as an effective treatment choice for a reduction of the possibility of infections occurring in complex skeletal wounds.[20−22] However, PLGA is expensive, and the attachment of PLGA on a PEEK substrate is still poor.[2,7,22] Therefore, our group developed a surface modification with ZnO rodlike arrays on the surface of a PEEK disk. Using its high surface area and suitable microstructures on the PEEK substrate, the values of absorption for various types of antibiotic agents increased, and the drug concentration that was released from the PEEK sample with the surface modification of ZnO/antibiotic agent into the testing solution was maintained at a level greater than the minimum inhibition concentration required to inhibit the growth of 90% (MIC 90) for *S. aureus* in 96 h (4 days).[7] However, the dissolution of ZnO rodlike arrays was found in the phosphate buffer solution because of the acidic properties of these antibiotic agents attached on the surface of ZnO rodlike arrays.[23] The release of the Zn^{2+} ions into the human body may result in cell cytotoxicity and may also cause a fast release rate of the antibiotic agent into the human body. Similar problems caused by a high concentration of antibiotic agent in the human body will also appear. In order to reduce the dissolution of ZnO rodlike arrays on the PEEK substrate, a further process for the modification of these ZnO rodlike arrays must be carried out. In this study, we tried to develop a simple chemical deposition method for the coating of TiO_2 layers onto the surface of ZnO rodlike arrays on PEEK substrates. Using the high surface area of TiO_2/ZnO rodlike arrays and good resistance of TiO_2 against acidic properties of antibiotic agents in buffer solution, various types of antibiotic agents might be directly attached onto the surface of TiO_2/ZnO rodlike arrays without the dissolution of these ZnO rodlike arrays. A heterogeneous implant with low cost, high safety, and good antibacterial properties may be produced and applied in orthopedic treatments. An in vitro release rate measurement of the antibiotic agent from the sample into the buffer solution, inhibition zone tests, and an analysis of optical densities for *S. aureus* or *E. coli* were also performed to understand the antimicrobial activities of these TiO_2/ZnO/PEEK samples.

2. RESULTS AND DISCUSSION

In this study, we tried to prepare a PEEK disk using a 3D-printing method with FDM technology. Then, the TiO_2/ZnO core−shell rodlike arrays were grown onto the PEEK disk using a simple chemical bath deposition method. Using the stable and superhydrophilicity properties of the TiO_2 layer on the ZnO surface,[24] the release of Zn^{2+} ions from ZnO rodlike arrays into buffer solution may be avoided, and the amount of antibiotic agents loaded onto the TiO_2 surface may also increase. First, we used a differential scanning calorimeter (DSC, TA DSC 50) and thermogravimetric analyzer (TGA, TA TGA Q 50) to measure thermal properties of PEEK samples. Results of a PEEK sample using DSC and TGA are shown in Figure S1I,II, respectively. In Figure S1I, the melting point (T_m) and crystallization temperature (T_c) of the PEEK material were observed at 338.5 and 290.5 °C, respectively. These results agree well with the thermal properties of PEEK reported in the literature.[25,26] However, decomposition of the PEEK material was observed at a temperature higher than 580 °C, as shown in the TGA result in Figure S1II, which agrees well with the reports proposed in the literature.[25,27] Therefore, the nozzle temperature of the 3D-printing equipment has to be kept in the range 290.5−580 °C. As proposed in the study by Yang et al. (2017),[28] increasing the temperature of the heating nozzle and the holder for the PEEK substrate may increase its crystallinity and therefore improve its printing quality. Without the increase in the temperature of the heating nozzle and holder to an optimal temperature, it is difficult to obtain a uniform and compact PEEK disk. Therefore, we set the temperature of the heating nozzle to 370 ± 10 °C and that of the holder for our 3D printer to 250 °C in order to obtain a highly crystalline and uniform PEEK disk. After the 3D-printed PEEK sample was made, the ZnO rodlike arrays were then grown onto the surface of the PEEK substrate in order to increase the effective surface area for further application. The detailed growth parameters were the same as those in our previous study.[7] As in the report by Chen et al. (2019),[7] the decomposition of ZnO rodlike arrays was observed in buffer solution which may have a harmful influence in the human body due to Zn^{2+} ions released from ZnO. Therefore, a passivation layer must be coated onto the ZnO rodlike arrays to avoid the release of any Zn^{2+} ions from the sample into the

https://doi.org/10.1021/acsomega.1c06931
ACS Omega 2022, 7, 9559−9572

testing solution. A TiO_2 passivation layer was then directly grown onto the surface of the ZnO rodlike arrays. X-ray diffraction (XRD) patterns of PEEK, PEEK/ZnO, and PEEK/ZnO/TiO_2 samples are shown in Figure 1. The blue line

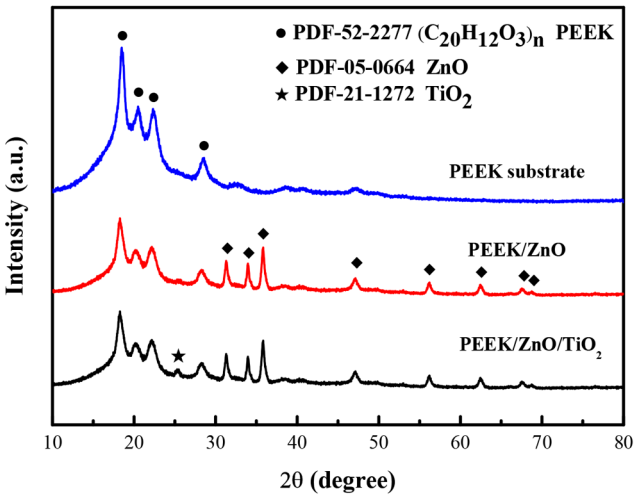

Figure 1. XRD patterns of samples prepared in this study.

shown in Figure 1 is the 3D-printed PEEK disk. Several peaks at 18.65°, 20.64°, 23.18°, and 28.92° are assigned to the crystal planes of (1 1 0), (1 1 1), (2 1 1), and (0 1 1), respectively, for the PEEK sample (JCPDS card 52-2277). For the PEEK/ZnO sample (red line in Figure 1), several extra peaks were observed compared to the XRD pattern of the PEEK sample. They are located at 31.74°, 34.48°, 36.22°, 47.48°, 56.54°, 62.78°, 66.30°, and 67.87°, which correspond to the crystal planes of (1 0 0), (0 0 2), (1 0 1), (1 0 2), (1 1 0), (1 0 3), (2 0 0), and (1 1 2) for wurtzite ZnO phase (JCPDS card 05-0664).

For the coating of TiO_2 passivation layers onto the surface of ZnO rodlike arrays (black line in Figure 1), a small peak at a 2θ of around 25° was observed, which corresponded to the anatase TiO_2 phase (JCPDS card 21-1272). It seemed that the low-crystalline anatase TiO_2 layer was coated on the PEEK/ZnO sample. Pan et al. (2019)[29] reported that a low-crystalline anatase TiO_2 layer was easily formed on the surface of a ZnO thin film using a sol−gel method. The phase diagram of TiO_2 proposed by Yamashita et al. (2018)[30] also shows a similar result. However, the results shown in Figure 1 only confirmed that the ZnO and TiO_2 samples could be grown onto the PEEK disk, but the microstructures of ZnO and ZnO/TiO_2 were still unknown. Therefore, a filed-emission scanning electron microscope (FE-SEM) was used to observe the surface microstructures of PEEK/ZnO and PEEK/ZnO/TiO_2 samples. The images of FE-SEM for PEEK/ZnO and PEEK/

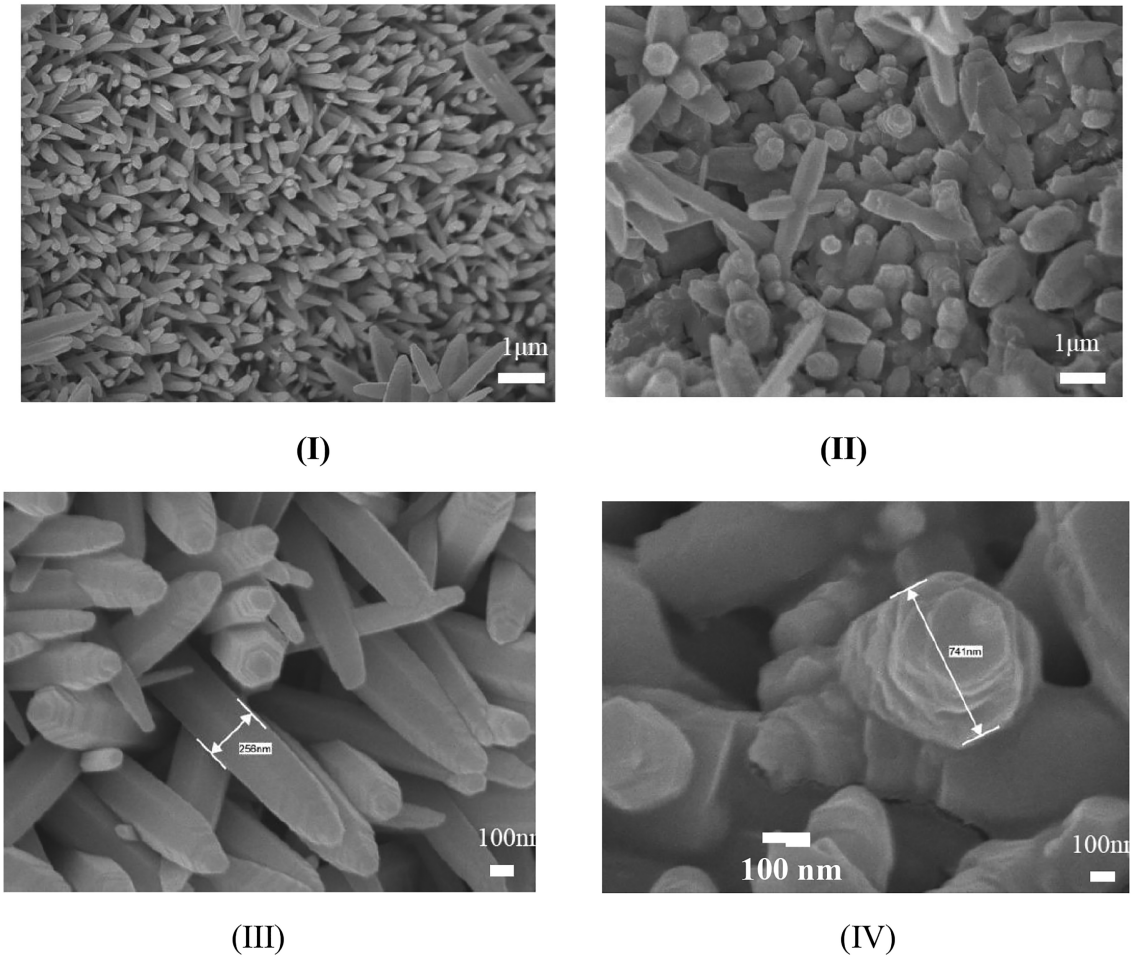

Figure 2. FE-SEM images of (I) ZnO and (II) ZnO/TiO_2 samples at 10K× and (III) ZnO and (IV) ZnO/TiO_2 samples at 50K×.

https://doi.org/10.1021/acsomega.1c06931
ACS Omega 2022, 7, 9559−9572

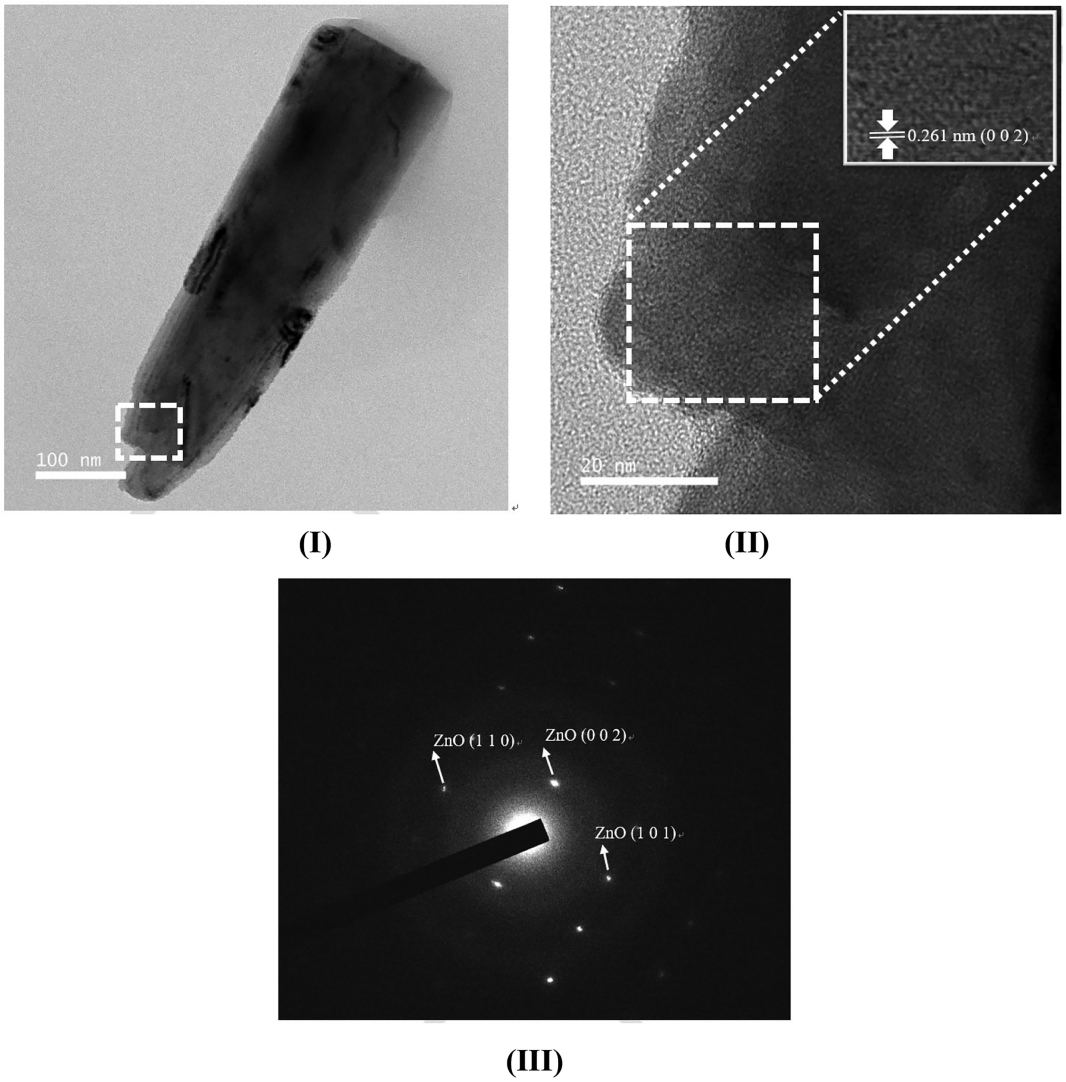

Figure 3. TEM images of ZnO/PEEK samples at (I) 80K× and (II) 600K× and (III) its SAED pattern.

ZnO/TiO_2 samples at 10K× are shown in Figure 2I,II, respectively.

In the FE-SEM image of the PEEK/ZnO sample (Figure 2I), hexagonal rodlike arrays were observed, which agreed well with our previous study.[7] In the FE-SEM image of the PEEK/ZnO sample with TiO_2 as the passivation layer (Figure 2II), a larger diameter of the rodlike arrays was found, which may be due to the coating of a TiO_2 passivation layer onto the ZnO surface. Figure 2III,IV shows the FE-SEM images for PEEK/ZnO and PEEK/ZnO/TiO_2 samples at 50K×, respectively. For the results given in Figure 2III,IV, the diameters of ZnO and TiO_2/ZnO rodlike microstructures were 256 and 741 nm, respectively. The increase in the diameter of the TiO_2/ZnO rodlike microstructure is due to the TiO_2 passivation layer coated onto the ZnO rodlike microstructure.

The compositions and distributions of samples are also important factors for further applications. An energy-dispersive spectroscopy (EDS) analysis of samples was then carried out with a working distance of 15 mm and acceleration voltage of 15 kV. The EDS results for PEEK/ZnO and PEEK/ZnO with TiO_2 as the passivation layer are shown in Figure S2I,II, respectively. The EDS spectra of PEEK/ZnO and PEEK/ZnO/TiO_2 showed that zinc and oxygen and zinc, oxygen, and titanium element spectra were clearly detected. The weight percentages of zinc, oxygen, and titanium elements were converted into atomic percentages for these elements. The atomic ratio of Zn:O in PEEK/ZnO samples is 47.52:52.48, which indicated that some zinc vacancies formed in the ZnO rodlike arrays. For the PEEK/ZnO/TiO_2 sample, the atomic ratio of zinc, oxygen, and titanium elements is 24.48:58.53:16.99, which indicated that the Ti element was deposited onto the ZnO surface. Figure S2III shows the mapping results of zinc and titanium elements in the PEEK/ZnO/TiO_2 sample. The mapping results indicated that uniform distributions of zinc and titanium elements were observed for the PEEK/ZnO/TiO_2 sample. However, the XRD, FE-SEM images, and EDS results showed that the TiO_2 passivation layer was coated onto the surface of ZnO rodlike structures. Evidence for the TiO_2/ZnO core−shell microstructures in the PEEK sample is still not enough. High-resolution transmission electron microscopy (TEM) was employed to examine properties of single ZnO and the TiO_2/ZnO rodlike microstructure, respectively. Figure 3I shows the TEM image of a single ZnO rodlike microstructure at 80K×. A ZnO rodlike microstructure can be clearly observed. Figure 3II shows the high-resolution TEM image

https://doi.org/10.1021/acsomega.1c06931
ACS Omega 2022, 7, 9559−9572

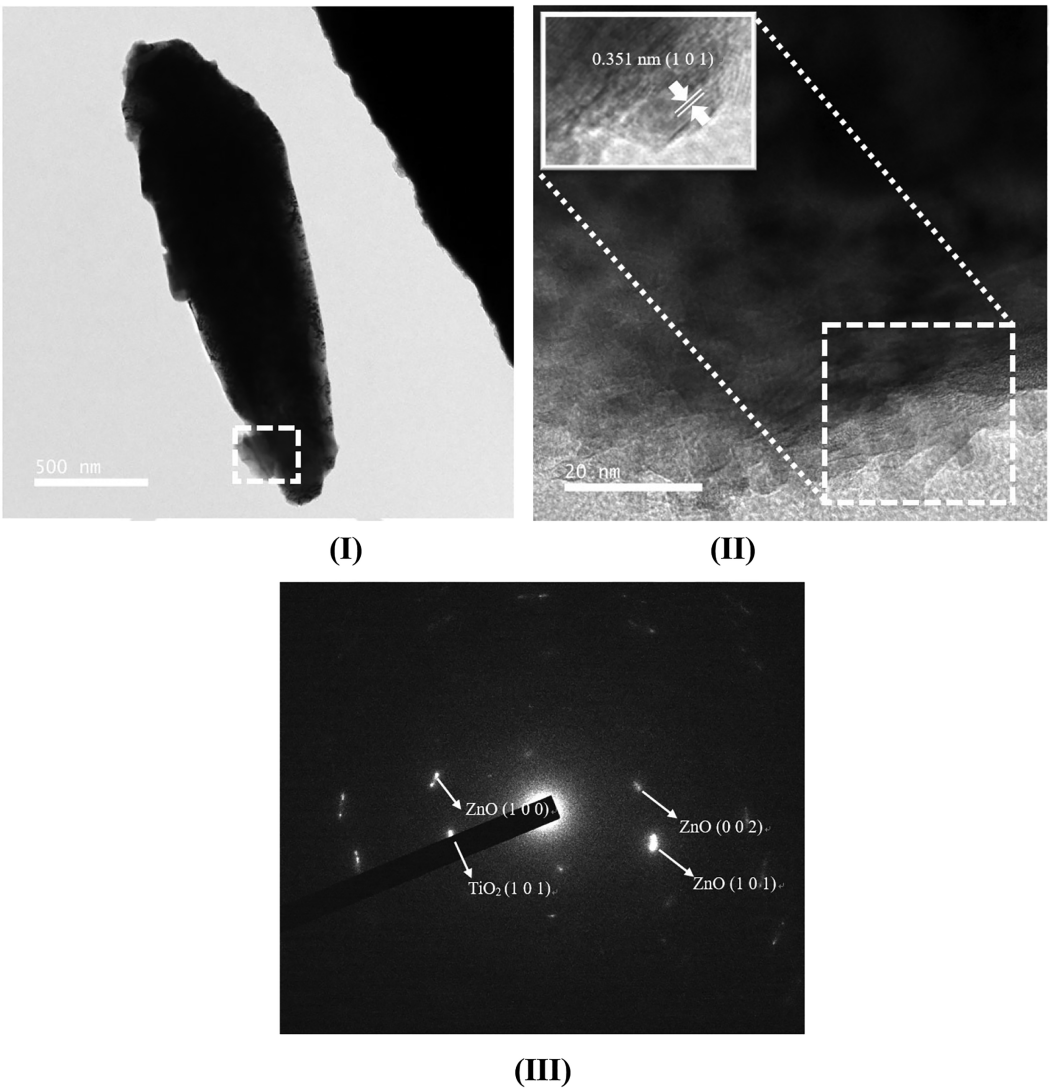

Figure 4. TEM images for ZnO/TiO_2/PEEK samples at (I) 80K× and (II) 600K× and (III) its SAED pattern.

of a local region of the single ZnO rodlike microstructure shown in Figure 3I at 600K×, and the inset in Figure 3II is the local region of the TEM image for the ZnO rodlike microstructure at 800K×. An interplanar space of around 0.261 nm is observed, which is consistent with a (0 0 2) crystal plane for ZnO. Figure 3III shows the corresponding selected area electron diffraction (SAED) pattern of the single ZnO rodlike microstructure. The SAED pattern agrees well with wurtzite ZnO phase spots, which is in agreement with the XRD patterns in Figure 1.

Figure 4I shows the TEM image of a single ZnO/TiO_2 rodlike microstructure at 80K×. A ZnO/TiO_2 rodlike microstructure can also be clearly observed and agrees well with the FE-SEM images reported in Figure 2. Figure 4II shows the high-resolution TEM image of a local region of the single ZnO/TiO_2 rodlike microstructure shown in Figure 4I at 600K×, and the inset in Figure 4II is the local region of the TEM image for a single ZnO/TiO_2 rodlike microstructure at 800K×. An interplanar space of around 0.351 nm is observed, which is consistent with the (1 0 1) crystal plane for the anatase TiO_2 phase.[31,32] Figure 4III shows the corresponding SAED pattern of a single ZnO/TiO_2 rodlike microstructure. Its SAED pattern agrees well with the wurtzite ZnO and anatase TiO_2 phase spots, which are also in agreement with the XRD pattern shown in Figure 1. Therefore, we can conclude that ZnO rodlike arrays with a TiO_2 passivation layer on a PEEK disk can be directly obtained using simple chemical bath deposition.

For possible applications of the direct attachment of antibiotic agents onto the surface of a PEEK/ZnO/TiO_2 sample, its surface area is an important factor that influences the absorption amount of antibiotic agent in a water bath. Therefore, a specific surface area analyzer was used to observe its active surface area. The absorption curves of ZnO and ZnO/TiO_2 rodlike arrays obtained from a specific surface area analyzer agreed well with type II absorption isothermal curves. Type II absorption isothermal curves of samples indicate multilayer absorption taking place at the sample surface.[33] The absorption between the sample and nonpolar gas (N_2 gas) involves the formation of many molecular layers on the surface rather than a single one. Using these absorption curves of samples, the effective surface area values for the PEEK/ZnO and that for TiO_2 as the passivation layer are around 1.42 and 1.13 m^2/g, respectively. With the coating of a TiO_2 passivation

https://doi.org/10.1021/acsomega.1c06931
ACS Omega 2022, 7, 9559−9572

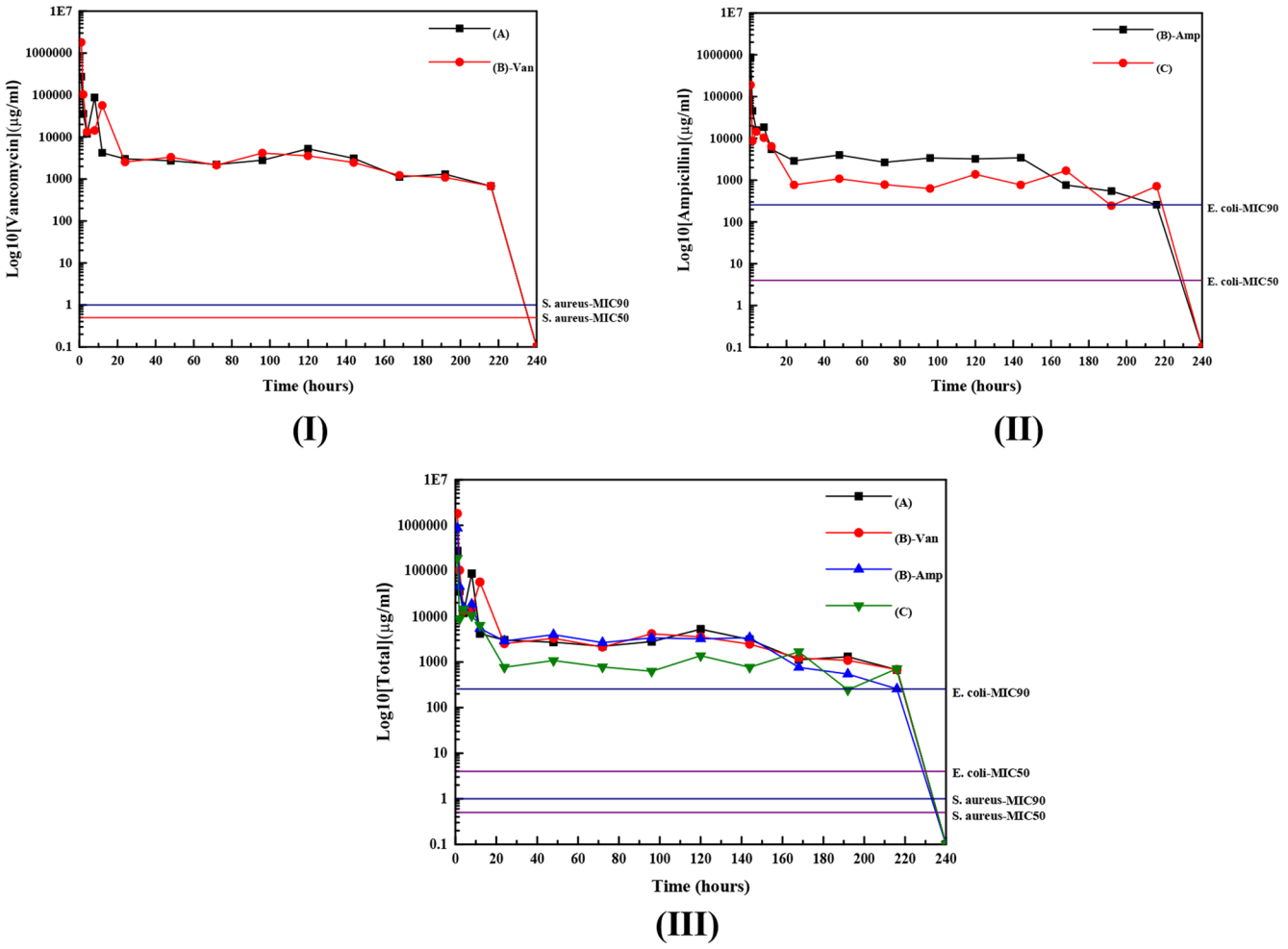

Figure 5. Release profile curves of (I) vancomycin salt, $p > 0.05$; and (II) ampicillin salt, $p > 0.05$. (III) Summary of various antibacterial agents released from samples into buffer solution as a function of time.

layer onto ZnO rodlike arrays, the effective surface area decreased compared with pristine ZnO rodlike arrays. The smaller value of the effective surface area for the PEEK/ZnO/TiO_2 sample indicated that the total area of the sample for physical absorption with nonpolar compounds decreased, and it may also reduce the amount of physical absorption for antibiotic agents in a water bath; however, it may also avoid the release of Zn^{2+} ions into human body.

Though we have reduced the possibility of Zn^{2+} released from the PEEK substrate with the TiO_2 passivation layer, its antibacterial property is still a problem. In order to avoid overuse in the local delivery of a high concentration of a drug in the human body, an improvement of the antibacterial property for PEEK implants is thus necessary. In this study, we prepared three types of antibiotic agent solutions for the direct absorption of drugs onto PEEK/ZnO/TiO_2 samples and evaluated their antibacterial properties. Sample A is a PEEK/ZnO/TiO_2 sample with the direct absorption of vancomycin salt in a water bath (20 mL of 50 mg/L antibiotic agent solution). Sample B is a PEEK/ZnO/TiO_2 sample with the direct absorption of an aqueous mixture containing vancomycin and ampicillin salts (20 mL of 25 mg/L vancomycin and 25 mg/L ampicillin salts). Sample C is a PEEK/ZnO/TiO_2 sample with the direct absorption of ampicillin salt in a water bath (20 mL of 50 mg/L antibiotic agent solution). Samples A and C are PEEK/ZnO/TiO_2 samples with the direct absorption of 100% of one antibiotic agent, and Sample B is a PEEK/ZnO/TiO_2 sample with the direct attachment of two kinds of antibiotic agents with a weight percentage of 50/50 w/w. The design reason for sample B is to decrease the amount of individual antibiotic agent loading on the sample but to maintain a suitable antimicrobial activity on both Gram-negative and Gram-positive bacteria. The decrease in the amount of each antibiotic agent may also reduce their possible influences on the human body and environmental pollution. The cost of implants may also reduce because the cost of vancomycin salt is much higher than that of ampicillin salt. After the direct absorption of a suitable amount of antibiotic agent by the sample in a water bath for 5 days, we could evaluate the weight percent of antibiotic agent absorbed onto the samples by the change in antibiotic agent concentrations in the water bath before and after the absorption process. The absorption percentages of antibiotic agent for samples A and C are 93.1% and 89.6%, respectively. The absorption percentage of the antibiotic agent mixture for sample B is 91.6% (the ratio for vancomycin and ampicillin salt absorbed onto sample was around 1:0.82). For the coating of the TiO_2 layer onto ZnO rodlike arrays, the absorbed amount of vancomycin salt is a little higher than that of ampicillin salt, which is the same result as in our previous study.[7] A possible reason may be more

https://doi.org/10.1021/acsomega.1c06931
ACS Omega 2022, 7, 9559−9572

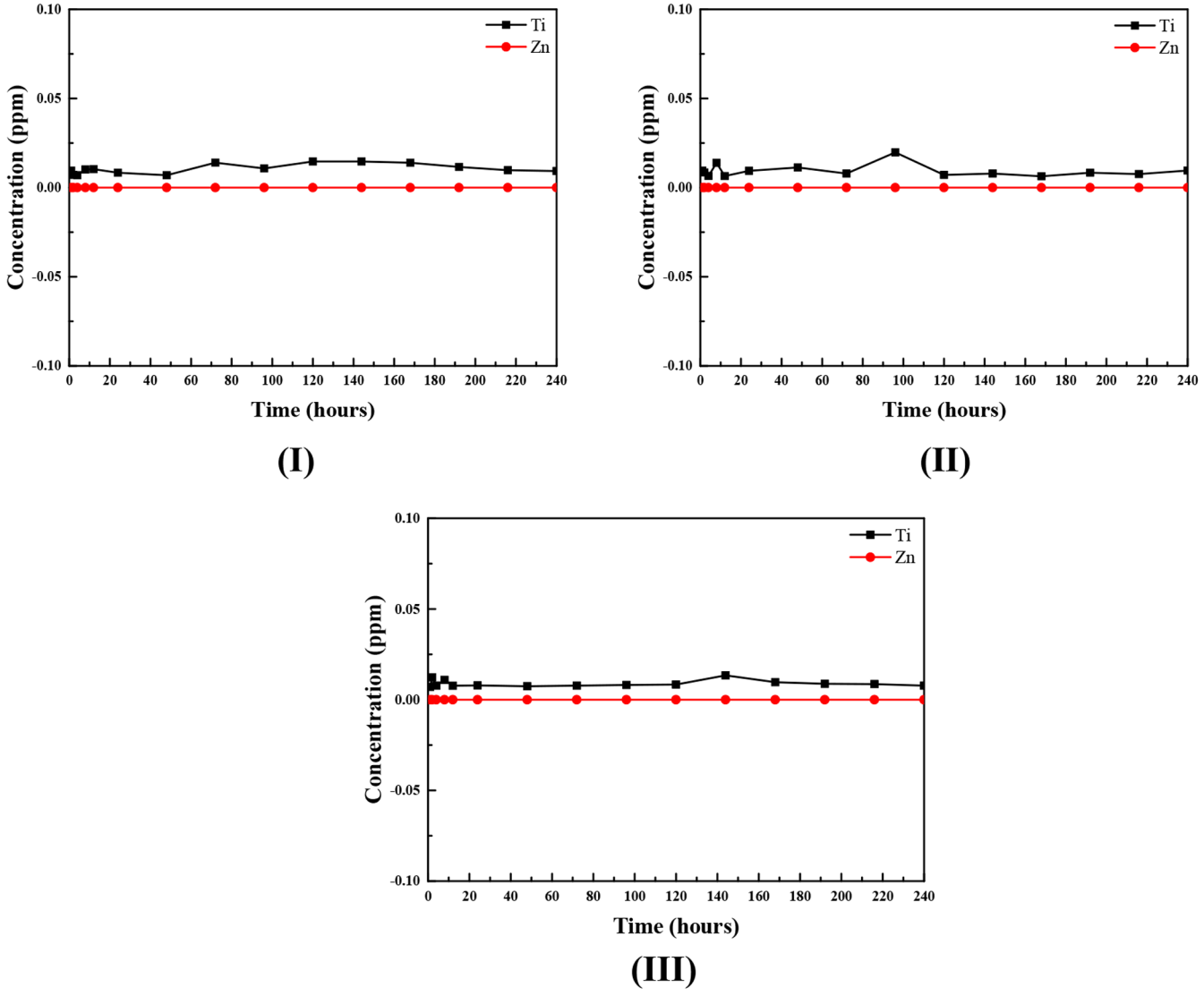

Figure 6. Variations of concentrations for Zn and Ti ions in buffer solutions for (I) sample A, (II) sample B, and (III) sample C as a function of time.

hydroxyl groups in the vancomycin salt compared with the ampicillin salt. For the absorption isothermal curve of the ZnO/TiO_2 sample, a type II absorption curve was observed, which indicated that the multilayer absorption of nonpolar compounds (N_2 gas) was taking place at the sample surface. However, it is well-known that the superhydrophilic property of the TiO_2 layer is observed due to the formation of hydroxyl groups on the TiO_2 surface.[24] These hydroxyl groups formed on the surface of the TiO_2 layer generate hydrogen bond interactions between the antibiotic agents and the TiO_2 surface and therefore make the total amount of absorption for vancomycin salt attached onto the sample surface a little greater than that for ampicillin, but the difference is not too large. For sample B, a similar tendency for the amount of drug attached on the sample was also observed. The next experiment is to evaluate the drug release behavior from the sample moving into the phosphate solution in order to estimate antimicrobial activities. In the report proposed by Sun et al. (2018),[34] the release of bone morphogenetic protein-2 (BMP-2) from the sulfonated PEEK substrate into the buffer solution is a rapid release process, which indicated that the good attachment and stable release profile of drugs are difficult without any surface modification of the PEEK substrate. Figure 5 shows the drug release curves for various kinds of antibiotic agents from samples into buffer solution. It is well-known that vancomycin salt has a good antibacterial performance on *S. aureus*, and the ampicillin salt has a good antibacterial performance on *E. coli*. Figure 5I shows the release curves of vancomycin salt from samples A and B (mixture of vancomycin salt/ampicillin salt of 50:50 in the solution bath for absorption) into phosphate solution. At 24 h, fast drops in the concentrations of vancomycin salt from samples A and B into the phosphate solution were observed. The release concentration of vancomycin salt in phosphate solution for sample A was a little greater than that for sample B at the first 24 h test because of the total influence of the interaction and the absorption amount of vancomycin salt at the surfaces of samples. The total absorption amount of vancomycin salt in sample A (100% of vancomycin salt in the solution) is much higher than that in sample B (50% of vancomycin salt in the solution); the possible release amount of vancomycin salt from sample A is therefore higher than that from sample B.

https://doi.org/10.1021/acsomega.1c06931
ACS Omega 2022, 7, 9559−9572

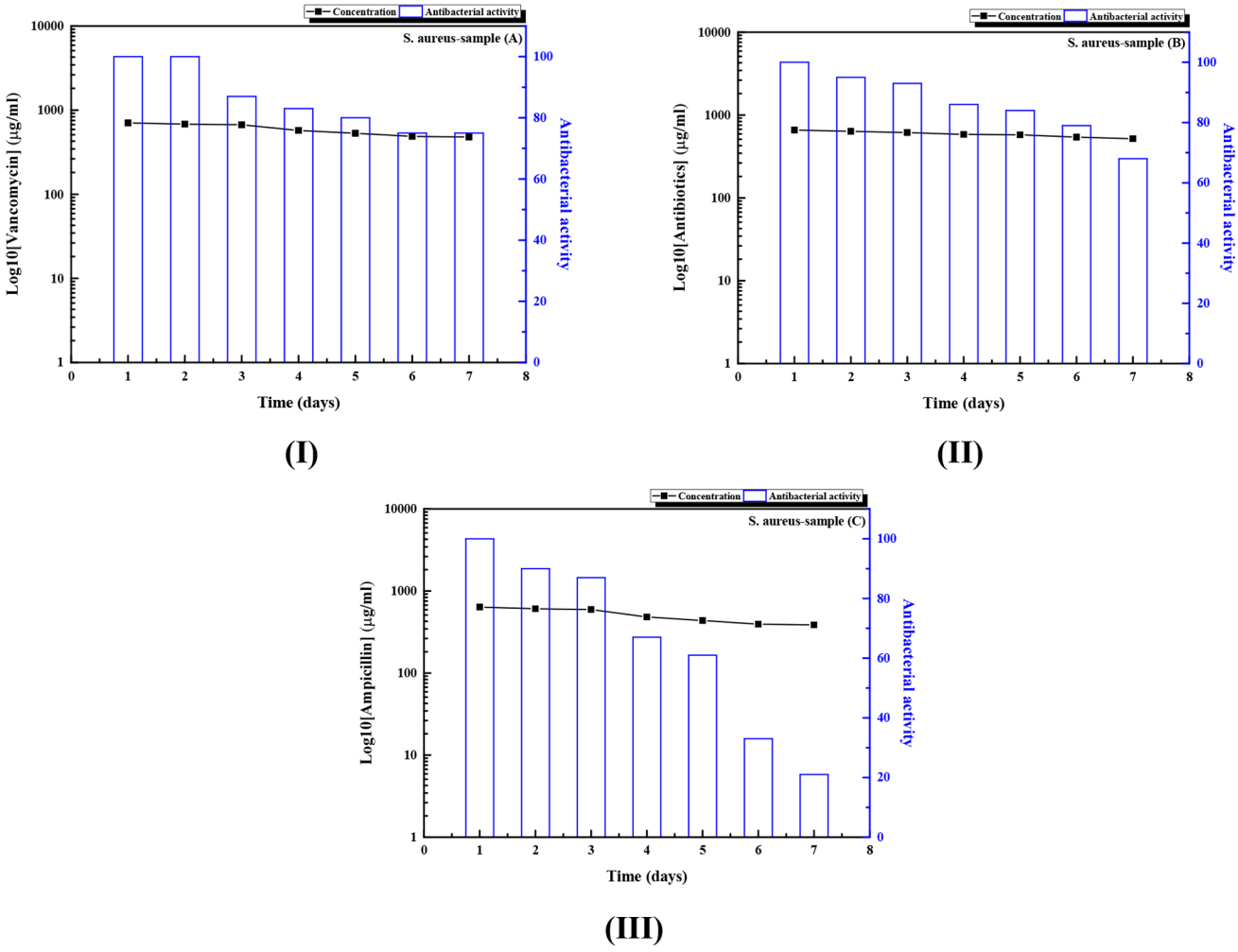

Figure 7. Antibacterial properties of *S. aureus* for (I) sample A, (II) sample B, and (III) sample C as a function of time. Statistical analyses of $p > 0.05$ for samples A and B and $p < 0.05$ for samples B and C.

According to the two-film theory,[35] the release rate of antibiotic agent from a sample into buffer solution is influenced by the difference between the concentration of antibiotic agent on the sample surface and that in the buffer solution. Theoretically, the release rate of vancomycin salt from sample A is around 2 times higher than that from sample B in the first testing period. However, hydrogen bonds formed between the TiO_2 surface and vancomycin salt resulted in the decrease in the release rate of vancomycin salt into buffer solution and therefore made the concentration of vancomycin salt for sample A in buffer solution a little higher than that for sample B in the first 24 h. Then, the stable concentrations of drug release profiles for vancomycin salt absorbed onto samples A and B were observed in the test time interval 24−240 h. After around 240 h (10 days), the amount of vancomycin salt in the buffer solution decreased and became lower than the value of MIC 90 for *S. aureus*,[36] which indicated that the good antibacterial performances of samples A and B for the inhibition of the growth of 90% *S. aureus* could be maintained for at least 10 days. Compared with our previous study,[7] we can extend their antibacterial performance on *S. aureus* from 4 days to 10 days. Figure 5II also reports the release profiles of ampicillin salt from samples B (mixture of vancomycin salt/ampicillin salt of 50:50 in a solution bath for absorption) and C into buffer solution. At 10 h, fast drops in the concentrations of ampicillin salt in phosphate solution for samples B and C were observed. The release amount of ampicillin salt in buffer solution for sample C was higher than that for sample B in the first 10 h test because of the high concentration of ampicillin salt in the water bath for the absorption onto sample C. One possible reason is the same as what we discussed before. The stable concentrations of drug release profiles for ampicillin salt absorbed onto samples B and C were observed in the test time interval 20−240 h. Also, after the test at around 240 h (10 days), the concentration of ampicillin salt in the phosphate solution decreased and become lower than the value of MIC 90 for *E. coli*,[37] which indicated that the antibacterial performances of samples B and C for the inhibition of the growth of 90% on *E. coli* could remain for at least 10 days. We also found that the variation of concentration for ampicillin released from sample C is higher than that from sample B. From the results reported in Figure 5I,II, we observed that the existence of vancomycin salt could make stable the release profile of ampicillin salt from sample B into buffer solution and control its antibacterial property to be higher than MIC 90 on both *S. aureus* and *E. coli*, which are Gram-negative and Gram-positive bacteria, respectively. From the results of a statistical analysis, a comparison of release

https://doi.org/10.1021/acsomega.1c06931
ACS Omega 2022, 7, 9559−9572

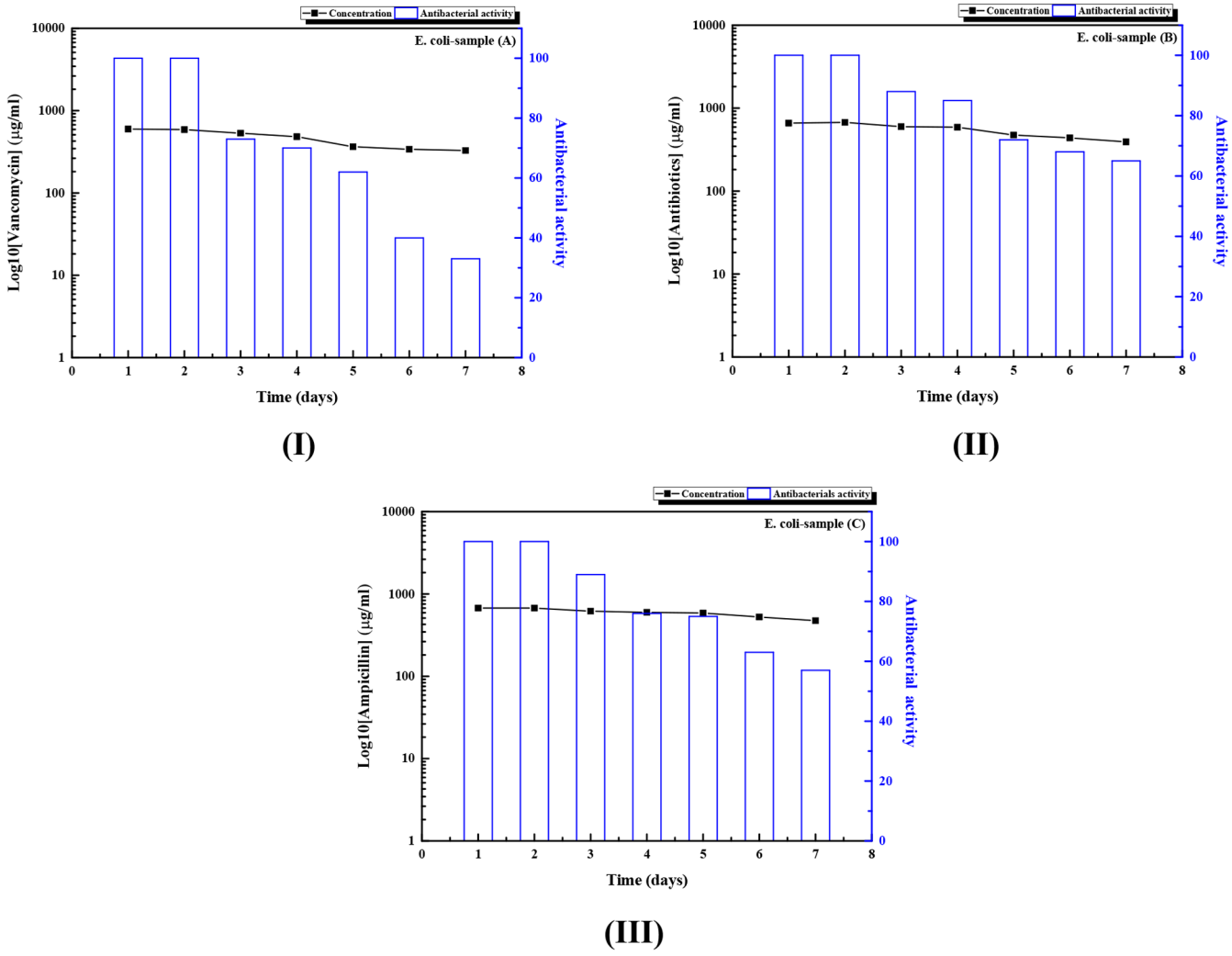

Figure 8. Antibacterial properties of *E. coli* for (I) sample A, (II) sample B, and (III) sample C as a function of time. Statistical analysis of $p < 0.05$ for samples A and B and $p > 0.05$ for samples B and C.

profiles for samples A and B in 10 days showed no statistically significant difference ($p > 0.05$). A similar statistical result was also observed from the comparison of release profiles for samples B and C in 10 days ($p > 0.05$). Although no statistical significances were observed from the results shown in Figure 5, we can still conclude that sample B may have a good antibacterial performance on both Gram-negative and positive bacteria and also reduce the individual damage of antibiotic agents on the human body and environmental pollution. Figure 5III shows the summary of drug release profiles for samples A−C. It indicated that their antibacterial performances may remain for at least 10 days.

In our previous study,[7] we observed that the decomposition of ZnO rodlike arrays occurred in the phosphate buffer solution after the 4 day test due to the acidic properties of ampicillin and vancomycin salt. The release of Zn^{2+} ions into buffer solution may have a harmful influence on the human body. Therefore, we examined the ionic concentrations of Zn^{2+} and Ti^{4+} ions in the phosphate buffer solution as a function of time. Figure 6 shows the variations of Ti^{4+} and Zn^{2+} ions in phosphate solution for samples A−C using an inductively coupled plasma optical emission spectrometry (ICP-OES) analysis. The concentrations of Ti^{4+} ions for all samples in buffer solution are lower than 0.025 ppm, and the concentrations of Zn^{2+} ions are almost zero in the 10 day test, which indicates that we can avoid the decomposition of ZnO rodlike arrays in the buffer solution when the antibiotic agents are loaded onto the samples. Low release concentrations of metal ions in buffer solution can increase their safety in applications of orthopedic treatments. Since we have tested the drug release profiles of various kinds of drugs attached onto the sample surface, the results show that all samples can release the drugs at concentrations greater than the values of MIC 90 on *S. aureus* and *E. coli*. However, antibiotic agents at a concentration higher than MIC 90 of organisms did not indicate that these samples had good antibacterial properties. Therefore, we also tested their antibacterial performances using a traditional disk diffusion method.

Figure 7I−III shows the antibacterial properties and the calculation of drug release distributions of different kinds of drugs in Petri dishes as a function of time using the calibration curve for the inhibition of *S. aureus*. For sample A (100% vancomycin salt in a water bath for absorption onto the sample surface, Figure 7I), its antibacterial property of higher than 80% on *S. aureus* can be maintained for at least 3 days and

https://doi.org/10.1021/acsomega.1c06931
ACS Omega 2022, 7, 9559−9572

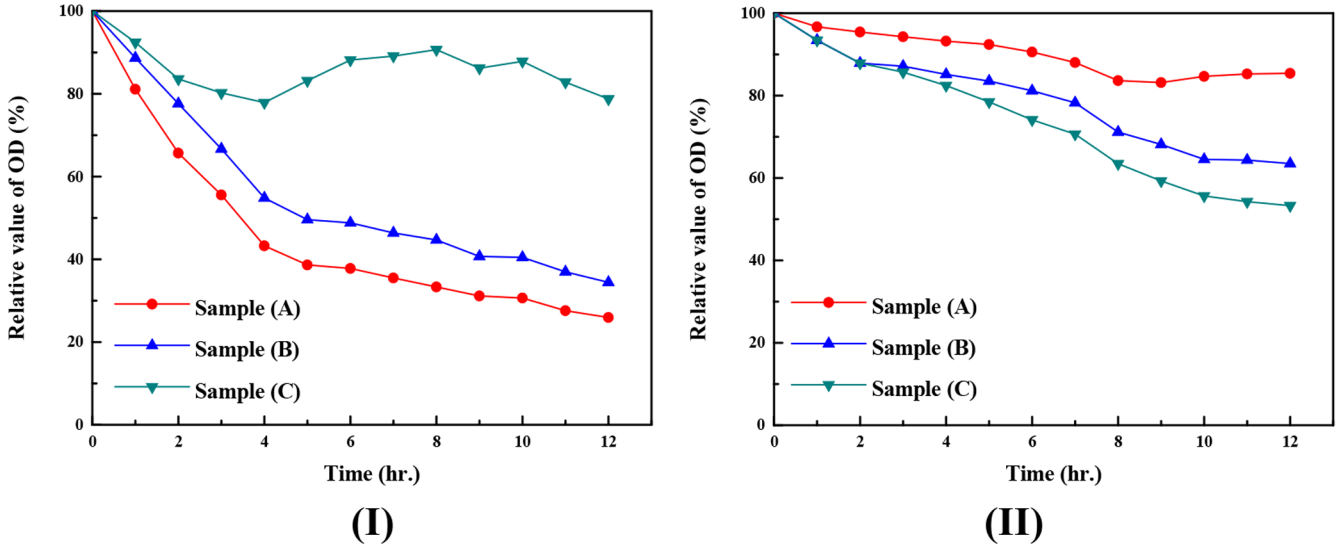

Figure 9. Optical density results for (I) *S. aureus* (statistical analysis: sample A with sample B, $p > 0.05$; sample B with sample C, $p < 0.05$) and (II) *E. coli* (statistical analysis: sample A with sample B, $p < 0.05$; sample B with sample C, $p > 0.05$) for various samples in a solution bath.

decreased to around 70% after the 7 day test. The antibacterial property of sample A estimated from the drug release distribution of antibiotic agent corresponded to the paper with the absorption of a standard concentration of vancomycin salt with a concentration of 600−700 μg/mL. For sample C (100% ampicillin salt in a water bath for absorption onto the sample surface, Figure 7III), its antibacterial property on *S. aureus* of higher than 80% can be maintained in the first 3 days and decrease in the 4−5 day test. After the 6 day test, its antibacterial property on *S. aureus* decreased to around 34% and approached 20% at the 7 day test. The antibacterial property of sample C estimated from the drug release distribution of antibiotic agent corresponded to the paper with the absorption of a standard concentration of ampicillin salt with a concentration of 700−500 μg/mL. With the results shown in Figure 7III, we can conclude that the effective bioactivity of ampicillin salt loaded on the TiO_2 sample decreases very fast. For sample B (50% vancomycin salt and 50% ampicillin salt in the solution bath, Figure 7II), its antibacterial property can remain higher than 80% in the first 6 day test. It decreased to 70% at the 7 day test. Sample B had a relatively longer and better antibacterial property on *S. aureus* than sample A and a much better antibacterial property on *S. aureus* than sample C. It is well-known that the antibacterial property of vancomycin salt on *S. aureus* is much better than that of ampicillin salt. Our study agrees well with this result.

According to our previous study,[2,7,20] we tested various loading ratios of vancomycin salt and ampicillin salt with PLGA as the control-release unit of the antibiotic agents from the ZnO surface into buffer solution. The results showed that the loading ratio of 50:50 for vancomycin and ampicillin salts on the ZnO sample has the best antibacterial activity on *S. aureus*. For the high loading ratio of vancomycin salt, good antibacterial properties on *S. aureus* for samples were observed in the first testing day, but the dissolution of ZnO caused by the high pK_a value for vancomycin salt made it lose its antibacterial property on *S. aureus* on the 4th day. A high loading ratio of ampicillin salt on ZnO rodlike arrays had a poor antibacterial property on *S. aureus* although a relatively low amount of dissolution for ZnO rodlike arrays was observed. With the loading ratio of 50:50 for vancomycin and ampicillin salts on the ZnO sample, the antibacterial property on *S. aureus* for the sample can be maintained for more than 4 days, but the time period with this antibacterial property of the sample was not enough. Also, we did not test its antibacterial property on *E. coli* with a loading ratio of 50:50 for vancomycin and ampicillin salts on the sample. Therefore, we also tested the antibacterial properties of samples A−C on *E. coli*, and they are shown in Figure 8I−III, respectively. For sample A (100% vancomycin salt in a water bath for absorption onto the sample surface, Figure 8I), its antibacterial property of higher than 80% on *E. coli* can remain for at least 2 days and decreased to around 30% after the 7 day test. The antibacterial property of sample A estimated from the drug release distribution of antibiotic agent corresponded to the paper with the absorption of standard vancomycin salt with a concentration of 500−600 μg/mL. This indicated that the effective antibacterial property for sample A decreased although its estimated antibacterial property corresponded to a standard concentration of 500−600 μg/mL for vancomycin salt absorbed on the paper. For sample C (100% ampicillin salt in a water bath for absorption onto the sample surface, Figure 8III), its antibacterial property on *E. coli* of higher than 80% can remain during the first 3 days and decrease to 75% in the 4−5 day test. After the 6 day test, its antibacterial property on *E. coli* decreased to 65% and approached to 55% in the 7 day test. The antibacterial property of sample C estimated from the drug release distribution of antibiotic agent corresponded to the paper with the absorption of a standard concentration of 600−800 μg/mL for ampicillin salt. With the results shown in Figure 8III, we can conclude that the effective bioactivity of ampicillin salt loaded on the TiO_2 sample decreased. The results shown in Figures 7 and 8 indicate that the pure ampicillin and vancomycin salts loaded onto the ZnO/TiO_2 rodlike array surface showed a poor antibacterial property on *S. aureus* and *E. coli*, respectively. It is well-known that vancomycin salt has a good antibacterial property on *S. aureus*, and ampicillin salt has a good antibacterial property on *E. coli*.[2,7,22] Therefore, poor antibacterial properties on *S. aureus* and *E. coli* using ampicillin salt and vancomycin salt were

https://doi.org/10.1021/acsomega.1c06931
ACS Omega 2022, 7, 9559−9572

expected. For sample B (50% vancomycin salt and 50% ampicillin salt in the solution bath for absorption, Figure 8II), the antibacterial property of sample B on *E. coli* can remain higher than 80% in the first 4 day test. It decreased to 65% at the 7 day test. Sample B had a relatively longer and better antibacterial property on *E. coli* than sample C and a much better antibacterial property on *E. coli* than sample A. These results also agree well with results shown in the literature.[2,7,20] Upon a statistical analysis, the antibacterial activity of sample A with sample B and sample B with sample C in 7 days did not show enough statistical significance ($p > 0.05$). From the results shown in Figures 7 and 8, we can still observe that sample B has a good antibacterial property on both *S. aureus* and *E. coli*.

The relatively low concentration of individual antibiotic agent may lead to low toxicity and environmental pollution during treatments of biomedical waste. The observations of the values of optical density on *S. aureus* and *E. coli* in the solutions with drugs attached onto the samples were also carried out for an understanding of their inhibition behavior on the growth of organisms.[2,7,38−40] With an increase in optical density value in the organism solution, the population of organisms in the solution increases; with a decrease in the optical density value, the growth of organisms in the solution is reduced. Figure 9I,II shows the relative optical density (OD) values for *S. aureus* and *E. coli* using samples A−C. The OD values of *S. aureus* in the same solution without the sample as a function of time were used as the standard test. For the concentration of *S. aureus* of around 10^8 colony-forming units (CFU)/mL (Figure 9I), the growth rates of *S. aureus* were inhibited with samples A and B in the solution. Sample C showed a relatively poor antimicrobial activity from the OD value observation in the solution. The inhibition of the growth rate of *S. aureus* with sample A is a little higher than that with sample B, but the difference is not too large. The statistical analysis for sample A with sample B showed no statistical significance $p > 0.05$. This may be due to the low concentration of vancomycin salt absorbed onto the sample B, and it may result in a relatively poor antibacterial property of sample B compared with sample A. For the concentration of *E. coli* of around 10^8 CFU/mL (Figure 9II), the growth rates of *E. coli* were inhibited with samples A−C in the solution. Sample C showed relatively better antimicrobial activities from the OD value observation in the solution, and sample A has a poor antibacterial property on *E. coli*. The inhibition of the growth rate of *E. coli* using sample B is a little lower than that for sample C, but the difference is not too large. The statistical analysis for sample B with sample C also showed no statistical significance $p > 0.05$. This may be due to the low concentration of ampicillin salt absorbed on sample B and result in a relatively poor antibacterial property of sample B compared with sample C. These results indicate that the direct absorption of the antibiotic agent mixture onto the TiO_2/ZnO rodlike array sample has good antimicrobial activity. The low release concentrations of Zn^{2+} ions from samples in buffer solution also indicate their good chemical resistances for corrosion applied in orthopedic surgery. The mixture of ampicillin/vancomycin in the solution bath with a suitable ratio for absorption onto the PEEK samples will be developed for biomaterials with long-term antibacterial properties of around 28 days, and an evaluation of their osteogenesis abilities will also be performed in the near future.

CONCLUSION

In this work, we reported a low-cost and simple process for the production of TiO_2/ZnO rodlike arrays on a PEEK disk for further applications in the biomaterial-related field. For the selection of 3D-printing parameters, the temperature of the nozzle in our 3D-printer was set at 370 ± 10 °C using the results of differential scanning calorimetry and thermogravimetric analysis. The 3D-printed PEEK disk was then used for the growth of TiO_2/ZnO rodlike arrays. XRD patterns and FE-SEM images of samples indicated that the TiO_2 layers can be grown onto the surface of ZnO rodlike arrays. TEM images of samples also confirmed these results. Therefore, various kinds of antibiotic agents loading onto the TiO_2/ZnO/PEEK samples can be produced using the direct absorption of different concentrations of antibiotic agents in a water solution. Around 90% of the antibiotic agents in the solution can be directly absorbed onto the samples during a 5 day absorption process. Stable antibiotic agent release profiles in the phosphate solution for samples were observed and led to concentrations of drugs in the buffer solution greater than those for MIC 90 on *S. aureus* and *E. coli* within 240 h. A suitable antibacterial property of the sample on *S. aureus* and *E. coli* with the loading of a mixture of ampicillin and vancomycin salts can be maintained for at least 7 days. The relatively low amount of individual antibiotic agent also leads to low cell cytotoxicity and environmental pollution. Relative values of optical density for *S. aureus* and *E. coli* in the solution with a concentration of 10^8 CFU/mL for organisms can decrease to 40% and 65% using the TiO_2/ZnO/PEEK sample with the loading of a mixture of vancomycin salt and ampicillin salt in 12 h. This study reported that a low-cost and simple technique for the production of PEEK/ZnO/TiO_2/antibiotic agent materials could have further applications in biomedical technology with almost zero concentration of metal ions released into the human body.

EXPERIMENTS

In this work, we grew ZnO rodlike arrays on a PEEK surface using chemical bath deposition. A TiO_2 layer was then coated onto the ZnO rodlike arrays in order to avoid the possible release of Zn^{2+} ions from the sample, which may be harmful during the application of PEEK implants. The detailed process for the 3D-printed PEEK disk is similar to those published in our previous study,[2,7] but the nozzle temperature of the 3D-printer was set at 370 ± 10 °C. The holder temperature of the PEEK sample using the 3D-printer was kept at 250 °C, and the printing speed of the 3D-printer was set at 10 mm/s for the preparation of the PEEK disk. After that, it was put into a Piranha solution (volume ratio of H_2SO_4/H_2O_2 = 3:1) with ultrasonic irradiation for 30 min. Then, the PEEK sample was put into deionized water with ultrasonic irradiation for 10 min. After these processes, the sample was cleaned by ethanol, deionized water, acetone, and deionized water several times and blown dry with ultrapure nitrogen gas.

The growth of ZnO rodlike arrays on the PEEK substrate was similar to the reports published in the literature.[7,41] A brief description is as follows: 0.5 mM potassium permanganate ($KMnO_4$, purity of greater than 99%, Aldrich Co.) with a volume of 10 mL and 25 μL of 1-butanol [$CH_3(CH_2)_3OH$, purity of greater than 99%, Alfa Aesar Co.] were mixed well and used for the activation solution for the PEEK disk in order generate Mn−hydroxyoxide on the PEEK surface. The PEEK

https://doi.org/10.1021/acsomega.1c06931
ACS Omega 2022, 7, 9559−9572

sample was put into the activation solution with a temperature of 85 °C and reaction time of 20 min. The PEEK disk was kept in the water bath with ultrasonic irradiation at a time interval of 10 min after the activation process. The apparatus for the growth of ZnO rodlike arrays on the PEEK disk is given in Figure S3. For ZnO rodlike arrays grown on a substrate, a mixture containing 2 mL of zinc nitrate [concentration of 1 M, $Zn(NO_3)_2{\cdot}6H_2O$, purity >98%, Sigma-Aldrich Co.], 3 mL of ammonium hydroxide (concentration of 5.5 M, NH_4OH, J. T. Baker Co.), 4 mL of 50% (v/v) ethanolamine (MEA, $NH_2CH_2CH_2OH$, purity of greater than 99%, Riedel-de Haën Co.), and deionized water with a volume of 11 mL was mixed well and put in a glass bottle. An activation PEEK substrate was directly moved into the glass bottle containing the reaction solution and kept in an oil bath with a temperature of 85 °C for 30 min to deposit the ZnO rodlike arrays onto the PEEK surface. After the growth of ZnO rodlike arrays on the PEEK surface, the sample was put in an oven at 70 °C with a time interval of 30 min. To coat TiO_2 thin films onto the surface of ZnO rodlike arrays, a reaction mixture containing 50 mL of absolute ethanol (Simga-Aldrich, purity >99.8%), 1 mL of tetrabutyl titanate ($C_{16}H_{36}O_4Ti$, Sigma-Aldrich, purity >99%), and 10 mL of deionized water with magnetic string for 30 min was prepared. Then, the PEEK/ZnO sample was put into this solution at 80 °C for 4 h to obtain the PEEK/ZnO/TiO_2 composite sample for the further absorption of different types of antibiotic agents.

The samples' crystal phases and their surface microstructures were analyzed using an X-ray diffractometer (XRD, D2 phaser, BRUKER, A26-X1-A2B0B2A) with Cu Kα (λ = 1.5418 Å) irradiation and a field-emission scanning electron microscope (FE-SEM, JEOL JSM-7500F), respectively. Their compositions and the values of effective surface area were also examined using an SEM instrument (S-3000N, Hitachi) connected to an energy-dispersive spectrometer (EDS, HORIBA, 7021-H) at an acceleration bias set at 15 kV and using a specific surface area analyzer (Micomeritics, ASAP 2020), respectively. Nitrogen gas for the measurement of the samples' surface area is employed with the pressure set at 3 μmHg. Because the specific surface area measurement for the sample is calculated using the amount of nitrogen gas absorbed at the sample surface, the sample has to be kept at the temperature of 90 °C to avoid any influence of water content in the sample. The ZnO/TiO_2 rodlike arrays on the PEEK substrate were also examined using a transmission electron microscope (TEM, JEOL JEM-2100 Plus). The TEM specimens were prepared by mechanically scratching on the ZnO/TiO_2 rodlike arrays at the substrate.

For the absorption of suitable concentrations of antibiotic agents on the surface of TiO_2/ZnO/PEEK disks, two types of antibiotic agents, which are ampicillin sodium salt ($C_{16}H_{18}N_3NaO_4S$, purity of greater than 98%, Aldrich Co.) and vancomycin hydrochloride ($C_{66}H_{75}Cl_2N_9O_{24}{\cdot}HCl$, purity of greater than 98%, Aldrich Co.), were used for the tests. The organisms for the inhibition zone tests were *S. aureus* (ATCC6538R) and *E. coli* (DH5α) provided from the Bioresource Collection and Research Center (BCRC, Taiwan). Nutrient Broth (NB, beef extract 3%, peptone 5g) was employed for the bioactivity tests on these organisms. The PEEK/TiO_2/ZnO/antibiotic agent sample was produced through the direct attachment of antibiotic agent on the surface of TiO_2/ZnO rodlike arrays on the PEEK disk. Concentrations of 50 mg/L pure vancomycin salt, 25 mg/L vancomycin salt and 25 mg/L ampicillin salt, and 50 mg/L pure ampicillin salt in aqueous solutions were employed for the absorption of the antibiotic agents onto the TiO_2/ZnO/PEEK samples. They are named samples A−C, respectively. An average area of around 1 cm^2 for the TiO_2/ZnO/PEEK sample was kept in the 20 mL aqueous solution containing a suitable amount of antibiotic agent for 5 days. After the absorption of antibiotic agent onto the sample surface was finished, the sample was maintained in a clean glass bottle to avoid any influence from outside chemicals or organisms.

An in vitro observation was carried out to understand the drug release profile from the sample into buffer solution. The approach was similar to those reported in our previous study.[2,7,23] 25 mL of the phosphate buffer solution (pH 7.4) was employed for the observation of release behavior for antibiotic agent from the sample into the buffer solution at 37 °C and a shaking rate of 30 rpm. An in vitro analysis test was carried out within a suitable time interval using UV−vis spectrophotometry (Varian Cary 50) and high-performance liquid chromatography (HPLC, Pu-2080, JASCO Co.) with a SYMMETRY C_8 column (4.6 × 250 mm, Shim-pack, VP-ODS). The buffer solution was replaced every test to avoid any possible influence caused by the saturated concentration of antibiotic agent in the solution bath. The detected wavelengths for ampicillin and vancomycin salt were 220 and 280 nm using the UV−vis spectrometer, respectively. They were also checked using HPLC. The concentrations of Zn^{2+} and Ti^{4+} ions in buffer solution were examined using inductively couple plasma optical emission spectrometry (Varian, Vista-Pro ICP-OES) to understand the possible dangers of cell toxicity for our samples.

The antibacterial property test for the samples was conducted similarly to that in our previous studies.[2,7,23] We seeded an *S. aureus* or *E. coli* inoculum with a volume of 200 μL in NB solution with a volume of 100 mL and grew organisms in 2.5 h at a temperature of 37 °C and a constant wavering rate of 220 rpm. The concentration of bacterial suspension solution was modified to around 10^8 CFU/mL. We used the antibiotic disk diffusion method for the examination of their antibacterial properties on *S. aureus* or *E. coli* in the agar containing NB in the Petri dish. 250 μL of organism solution with a bacterial concentration of 10^8 CFU/mL was seeded onto the agars in the Petri disks for the test. Their inhibition zone test was analyzed at 37 °C. A calibration curve for the inhibition zone of the organisms was also made using the paper with a loading of a standard concentration of each type of antibiotic agent (1, 10, 100, and 1000 μg/mL), separately. The concentration of antibiotic agent released from the sample was then calculated by interpreting these curves. The antibacterial property of the sample on organisms was determined by the following equation:

$$\text{antibacterial properties (\%)} = \frac{\text{diameter of sample inhibition zone}}{\text{diameter of maximum inhibition zone}} \times 100 \quad (1)$$

For the observation of the optical density of a solution containing the bacterial suspension and the samples, solutions with a concentration of bacterial suspension (10^8 CFU/mL) for the *S. aureus* and *E. coli* were used in order to estimate their antimicrobial activities (samples A−C). A standard examination with only organisms in the solution was also performed in order to estimate the growth rate of the organism as a function

https://doi.org/10.1021/acsomega.1c06931
ACS Omega 2022, 7, 9559−9572

of time. The solution containing the organism suspension was brought to 37 °C with a wavering rate of 180 rpm. The optical density values for these solutions containing an organism suspension with the drug attached onto the samples were analyzed using scanning spectrophotometry (Shimadzu, UV-1601PC) with the light wavelength set at 600 nm. The relative optical density value of the bacterial suspension solution was estimated using the following equation:

$$\text{relative value of OD (\%)} = \frac{\text{OD value of solution}}{\text{OD value of standard solution}} \times 100 \quad (2)$$

Statistical analyses of the experimental data for samples A and B and samples B and C were carried out. For our main analysis, we estimated a linear regression difference-in-differences model with a binary indicator for a change at the middle cutoff point, with time fixed effects. *P*-values were two-sided, and statistical significance was established at $p < 0.05$. All statistical analyses were performed using "Stata MP" (14.2, 1985−2015, StataCorp LLC, College Station, TX).

■ ASSOCIATED CONTENT

Supporting Information

The Supporting Information is available free of charge at https://pubs.acs.org/doi/10.1021/acsomega.1c06931.

Apparatus used for the growth of ZnO rodlike arrays on PEEK substrates; results for DSC and TGA measurements for PEEK substrates used in this study; and EDS results for PEEK/ZnO and PEEK/ZnO/TiO_2 samples and mapping results for Zn and Ti elements on the PEEK/ZnO/TiO_2 sample (PDF)

■ AUTHOR INFORMATION

Corresponding Authors

Dave W. Chen − *Department of Orthopedic Surgery, Chang Gung Memorial Hospital, Keelung Branch, Keelung 333, Taiwan; College of Medicine, Chang Gung University, Taoyuan 33302, Taiwan*; Email: mr5181@adm.cgmh.org.tw

Kong-Wei Cheng − *Department of Chemical and Materials Engineering, Chang Gung University, Taoyuan 33302, Taiwan; Department of Orthopedic Surgery, Chang Gung Memorial Hospital, Keelung Branch, Keelung 333, Taiwan*; orcid.org/0000-0002-7574-7200; Phone: +886-3-2118800-3353; Email: kwcheng@mail.cgu.edu.tw; Fax: +886-3-2118668

Authors

Ngi-Chiong Lau − *Department of Chemical and Materials Engineering, Chang Gung University, Taoyuan 33302, Taiwan; Department of Orthopedic Surgery, Chang Gung Memorial Hospital, Keelung Branch, Keelung 333, Taiwan; College of Medicine, Chang Gung University, Taoyuan 33302, Taiwan*

Yin-Cheng Lai − *Department of Chemical and Materials Engineering, Chang Gung University, Taoyuan 33302, Taiwan*

Complete contact information is available at: https://pubs.acs.org/10.1021/acsomega.1c06931

Author Contributions

The manuscript was written through contributions of all authors. All authors have given approval to the final version of the manuscript

Notes

The authors declare no competing financial interest.

■ ACKNOWLEDGMENTS

This work was sponsored by the Chang Gung Memorial Hospital, Keelung, grants CMRPG2L0131 and BMRP948. The authors thank the Chang Gung University Microscope Center for the SEM and TEM analyses.

■ REFERENCES

(1) Campbell, I.; Diegel, O.; Wohlers, O. K. *Additive manufacturing and 3D printing state of the industry annual worldwide progress report*; Wohlers Report; Wohlers Associates, 2018.

(2) Lau, N. C.; Tsai, M. H.; Chen, D. W.; Chen, C. H.; Cheng, K. W. Preparation and characterization for antibacterial activities of 3D printing polyetheretherketone disks coated with various ratios of ampicillin and vancomycin Salts. *Appl. Sci.* **2020**, *10*, 97.

(3) Singh, S.; Prakash, C.; Ramakrishna, S. 3D printing of polyether-ether-ketone for biomedical applications. *Eur. Polym. J.* **2019**, *114*, 234−248.

(4) Goole, J.; Amighi, K. 3D printing in pharmaceutics: A new tool for designing customized drug delivery systems. *Int. J. Pharm.* **2016**, *499*, 376−394.

(5) Norman, J.; Madurawe, R. D.; Moore, C. M. V.; Khan, M. A. A.; Khairuzzaman, A. A. new chapter in pharmaceutical manufacturing; 3D-pring drug product. *Adv. Drug Delivery Review* **2017**, *108*, 39−50.

(6) Stansbury, J. W.; Idacavage, M. J. 3D printing with polymers: Challenges among expanding options and opportunities. *Dental. Mater.* **2016**, *32*, 54−64.

(7) Chen, D. W.; Lee, K. Y.; Tsai, M. H.; Lin, T. Y.; Chen, C. H.; Cheng, K. W. Antibacterial applications on staphylococcus aureus using antibiotic agent/zinc oxide nanorod arrays/polyethylethylketone composite samples. *Nanomaterials* **2019**, *9* (5), 713.

(8) Kizuki, T.; Matsushita, T.; Kokubo, T. Apatite-forming PEEK with TiO_2 surface layer coating. *J. Mater. Sci. Mater. Med.* **2015**, *26* (1), 41.

(9) Chen, F.; Ou, H.; Gatea, S.; Long, H. Hot tensile fracture characteristics and constitutive modelling of polyether-ether-ketone (PEEK). *Polym. Test.* **2017**, *63*, 168−179.

(10) Anguiano-Sanchez, J.; Martinez-Romero, O.; Siller, H. R.; Diaz-Elizondo, J. A.; Flores-Villalba, E.; Rodriguez, C. A. Influence of PEEK coating on hip implant stress shielding: a finite element analysis. *Compute Math. Methods Med.* **2016**, *2016*, 6183679.

(11) Wu, J.; Li, L.; Fu, C.; Yang, F.; Jiao, Z.; Xhi, X.; Ito, Y.; Wang, Z.; Liu, Q.; Zhang, P. Micro-porous polyetheretherketone implants decorated with BMP-2 via phosphorylated gelatin coating for enhance cell adhesion and osteogenic differentiation. *Colloids Surf. B Biointerfaces* **2018**, *169*, 233−241.

(12) Parthasarathy, J. 3D modeling custom implants and its future perspectives in craniofacial surgery. *Ann. Maxillofac Surg.* **2014**, *4*, 9−18.

(13) Schmidt, M.; Pohle, D.; Rechtenwald, T. Selective laser sintering of PEEK. *CIRP Annals* **2007**, *56*, 205−208.

(14) Bakhshandeh, S.; Gorgin Karaji, Z.; Lietaert, K.; Fluit, A. C.; Boel, C. H. E.; Vogely, H. C.; Vermonden, T.; Hennink, W.; Weinans, H.; Zadpoor, A. A.; Amin Yavari, S. Simultaneous delivery of multiple antibacterial agents from additively manufactured porous biomaterials to fully eradicate planktonic and adherent staphylococcus aureus. *ACS Appl. Mater. Int.* **2017**, *9*, 25691−25699.

(15) Widmer, A. F. New developments in diagnosis and treatment of infection in orthopedic implants. *Clin. Infect. Dis* **2001**, *33*, S94−S106.

https://doi.org/10.1021/acsomega.1c06931
ACS Omega 2022, 7, 9559−9572

(16) Brown, T. S.; Petis, S. M.; Osmon, D. R.; Mabry, T. M.; Berry, D. J.; Hanssen, A. D.; Abdel, M. P. Periprosthetic joint infection with fungal pathogens. *J. Arthroplasty* **2018**, *33*, 2605−2612.
(17) Liu, J.; Ma, J.; Bao, Y.; Wang, J.; Zhu, Z.; Tang, H.; Zhang, L. Nanoparticle morphology and film-forming behavior of polyacrylate/ZnO nanocomposite. *Composites Sci. & Technol.* **2014**, *98*, 64−7127.
(18) Romanò, C. L.; Manzi, G.; Scarponi, S.; Logoluso, N.; George, D. Practice and guidelines for treating periprosthetic joint infections. In *Single- and two-stage revision, Management Periprosthetic Joint Infections*; Woodhead Publishing: Cambridge, 2017; pp 183−218.
(19) Hasan, J.; Crawford, R. J.; Ivanova, E. P. Antibacterial surfaces: the quest for a new generation of biomaterials. *Trends Biotechnol.* **2013**, *31*, 295−304.
(20) Chen, D. W.; Hsu, Y. H.; Liao, J. Y.; Liu, S. J.; Chen, J. K.; Ueng, S. W. N. Sustainable release of vancomycin, gentamicin and lidocaine from novel electrospun sandwich-structured PLGA/collagen nanofibrous membranes. *Int. J. Pharm.* **2012**, *430*, 335−341.
(21) Mi, F. L.; Lin, Y. M.; Wu, Y. B.; Shyu, S. S.; Tsai, Y. H. Chition/PLGA blend microspheres as a biodegradable drug-delivery system: Phase-separation, degradation and release behavior. *Biomaterials* **2002**, *23*, 3257−3267.
(22) Chen, C. H.; Yao, Y. Y.; Tang, H. C.; Lin, T. Y.; Chen, D. W.; Cheng, K. W. Long-term antibacterial performances of biodegradable polylactic acid materials with direct absorption of antibiotic agents. *RSC Adv.* **2018**, *8*, 16223−16231.
(23) Kang, M. A.; Kang, J. S. Stability test of ampicillin sodium solutions in the accufuser® elastomeric infusion device Using HPLC: UV method. *Pharmacol. Pharm.* **2012**, *3*, 462−467.
(24) Fujishima, A.; Rao, T. N.; Tryk, D. A. Titanium dioxide photocatalysts. *J. Photochem. & Photobio. C Photochem. Review* **2000**, *1*, 1−21.
(25) Venkatraman, P.; Rader, C.; Bohmann, N.; Foster, E. J. Structure-property-processing relationship of ethanol solvent exchanged PEEK. *Polymer* **2019**, *169*, 154−159.
(26) Tsafack, T.; Bartolucci, S. F.; Maurer, J. A. An atomistic view of heat propagation from graphene to polyetheretherketone (PEEK). *Compute Mater. Sci.* **2020**, *177*, 109590.
(27) Ajeesh, G.; Bhowmik, S.; Sivakumar, V.; Varshney, L.; Kumar, V.; Abraham, M. Investigation on polyetheretherketone composite for long term storage of nuclear waste. *J. Nucl. Mater.* **2015**, *467*, 855−862.
(28) Yang, C.; Tian, X.; Li, D.; Cao, Y.; Zhao, F.; Shi, C. Influence of thermal processing conditions in 3D printing on the crystallinity and mechanical properties of PEEK material. *J. Mater. Proce. Technol.* **2017**, *248*, 1−7.
(29) Pan, Y.; Liu, B.; Hu, H.; Jiang, H.; Wei, F.; Zhou, M.; Fan, X.; Yu, H.; Niu, G.; Huang, J. Preparation and photocatalytic performance of the rod-shaped Ni-NiO/TiO_2 hollow composite structure based on metallization cellulose fibers and TBOT. *Vacuum* **2019**, *159*, 1−8.
(30) Yamashita, Y.; Ishiguro, K.; Nakai, D.; Fuji, M. The synthesis of a porous-type of TiO_2 with rutile structure. *Adv. Powder Technol.* **2018**, *29*, 2521−2526.
(31) Aijo, J. K.; Manju, T.; Joaquim, P.; Anuroop, R.; Pradeep, B.; Thoudinja, S.; Rachel, R. P. Rapid room temperature crystallization of TiO_2 nanotubes. *CrystEngComm.* **2017**, *19*, 1585−1589.
(32) He, J.; Du, Y.; Bai, Y.; An, J.; Cai, X.; Chen, Y.; Wang, P.; Yang, X.; Feng, Q. Facile formation of anatase/rutile TiO_2 nanocomposites with enhanced photocatalytic activity. *Molecules* **2019**, *24*, 2996.
(33) Maron, S. H.; Lando, J. B *Fundamentals of Physical Chemistry*; Macmillan Publishing Co. Inc.: NY, 1974.
(34) Sun, Z.; Yang, L. O.; Ma, X.; Qiao, Y.; Liu, X. Controllable and durable release of BMP-2-loaded 3D porous sulfonated polyetheretherketone (PEEK) for osteogenic activity enhancement. *Colloids Surf., B* **2018**, *171*, 668−6741.
(35) Bird, R. B.; Stewart, W. E; Lightfoot, E. N *Transport Phenomena*; John Wiley & Sons, Inc.: NY, 1960.
(36) Khurana, S.; Mathur, P.; Malhotra, R. Staphylococcus aureus at an Indian tertiary hospital: antimicrobial susceptibility and minimum inhibitory concentration (MIC) creep of antimicrobial agents. *J. Global Antimicrobial Resist.* **2019**, *17*, 98−102.
(37) Hayami, H.; Takahashi, S.; Ishikawa, K.; Yasuda, M.; Yamamoto, S.; Wada, K.; Kobayashi, K.; Hamasuna, R.; Minamitani, S.; Matsumoto, T.; et al. Second nationwide surveillance of bacterial pathogens in patients with acute uncomplicated cystitis conducted by Japanese Surveillance Committee from 2015 to 2016: antimicrobial susceptibility of Escherichia coli, Klebsiella pneumoniae, and Staphylococcus saprophyticus. *J. Infection and Chemotherapy* **2019**, *25*, 413−422.
(38) Čepin, M.; Ovanovski, V.; Podlogar, M.; Orel, Z. C. Amino- and ionic liquid-functionalised nanocrystalline ZnO *via* silane anchoring − an antimicrobial synergy. *J. Mater. Chem. B* **2015**, *3*, 1059−1067.
(39) Malzahn, K.; Jamieson, W. D.; Dröge, M.; Mailänder, V.; Jenkins, A. T. A.; Weiss, C. K.; Landfester, K. Advanced dextran based nanogels for fighting *Staphylococcus aureus* infections by sustained zinc release. *J. Mater. Chem. B* **2014**, *2*, 2175−2183.
(40) Yang, J.; Zhang, X.; Ma, Y. H.; Gao, G.; Chen, X.; Jia, H. R.; Li, Y. H.; Chen, Z.; Wu, F. G. Carbon dot-based platform for simultaneous bacterial distinguishment and antibacterial applications. *ACS Appl. Mater. Int.* **2016**, *8*, 32170−32181.
(41) Kokotov, M.; Hodes, G. Reliable chemical bath deposition of ZnO films with controllable morphology fromethanolamine-based solutions using $KMnO_4$ substrate activation. *J. Mater. Chem.* **2009**, *19*, 3847−3854.

https://doi.org/10.1021/acsomega.1c06931
ACS Omega 2022, 7, 9559−9572